Metalloproteins

Deutsche Ausgabe: DOI: 10.1002/ange.201606447
Internationale Ausgabe: DOI: 10.1002/anie.201606447

The Nitrogenase FeMo-Cofactor Precursor Formed by NifB Protein: A Diamagnetic Cluster Containing Eight Iron Atoms

Yisong Guo[+], Carlos Echavarri-Erasun[+], Marie Demuez, Emilio Jiménez-Vicente, Emile L. Bominaar,* and Luis M. Rubio**

Abstract: *The biological activation of N_2 occurs at the FeMo-cofactor, a 7Fe–9S–Mo–C–homocitrate cluster. FeMo-cofactor formation involves assembly of a Fe_{6-8}–S_X–C core precursor, NifB-co, which occurs on the NifB protein. Characterization of NifB-co in NifB is complicated by the dynamic nature of the assembly process and the presence of a permanent [4Fe–4S] cluster associated with the radical SAM chemistry for generating the central carbide. We have used the physiological carrier protein, NifX, which has been proposed to bind NifB-co and deliver it to the NifEN protein, upon which FeMo-cofactor assembly is ultimately completed. Preparation of NifX in a fully NifB-co-loaded form provided an opportunity for Mössbauer analysis of NifB-co. The results indicate that NifB-co is a diamagnetic ($S=0$) 8-Fe cluster, containing two spectroscopically distinct Fe sites that appear in a 3:1 ratio. DFT analysis of the ^{57}Fe electric hyperfine interactions deduced from the Mössbauer analysis suggests that NifB-co is either a $4Fe^{2+}$–$4Fe^{3+}$ or $6Fe^{2+}$–$2Fe^{3+}$ cluster having valence-delocalized states.*

Mo-nitrogenase carries at its active site a complex cofactor, designated FeMo-co, composed of a [7Fe–Mo–9S–C] portion bound to homocitrate (Figure 1 A). FeMo-co biosynthesis occurs outside nitrogenase in a pathway involving a series of Nif proteins that act as substrate-providing enzymes, molecular scaffolds, or cluster carriers.[1] NifB catalyzes the first committed step in the pathway, that is, the conversion of [4Fe–4S] clusters into NifB-co, an Fe–S cluster of higher nuclearity with a central C atom that serves as precursor of FeMo-co in Mo-nitrogenase, of FeV-co in V-nitrogenase, and of FeFe-co in Fe-only nitrogenase.[2] Interestingly, NifB-co was purified before NifB,[3] and its role as FeMo-co precursor was unambiguously established by the transfer of ^{55}Fe and ^{35}S labels from NifB-co into FeMo-co.[4] NifB-co binds readily to NifEN, a nitrogenase-like molecular scaffold, and can be shuttled from NifB to NifEN by the metallocluster carrier protein NifX (Supporting Information, Figure S1).[5] The final stage of FeMo-co synthesis occurs in a NifEN/NifH complex.[6] Extended X-ray absorption fine structure (EXAFS) and nuclear resonance vibrational spectroscopy (NRVS) analysis of in vitro produced NifX-bound NifB-co (NifX/NifB-co) indicated that it comprised, at a minimum, the central [6Fe–9S–C] moiety of FeMo-co.[7] Herein, we purify an in vivo formed NifX/NifB-co complex and use Mössbauer spectroscopy and density functional theory (DFT) to investigate the Fe centers in NifB-co (Figure 1 B).

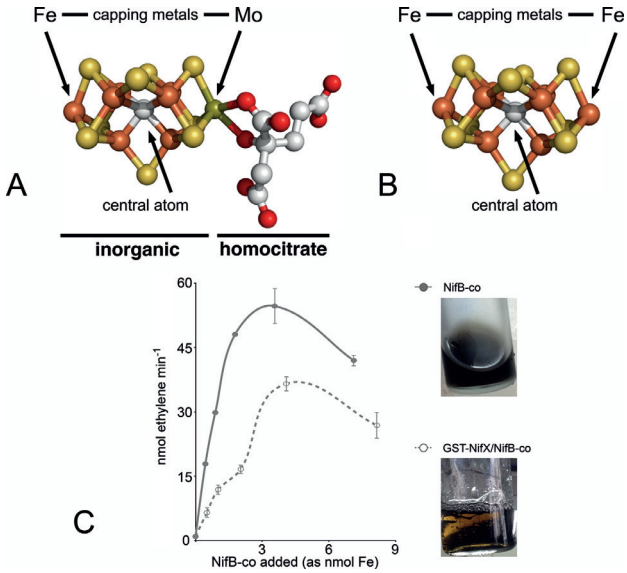

Figure 1. A) Structure of FeMo-co. B) [8Fe–9S–C] NifB-co structure proposed in this work. C) NifB-co dependent in vitro synthesis of FeMo-co and apo-nitrogenase activation with purified NifB-co (●) or NifX/NifB-co (○) samples. Top right: anaerobic vial with pure NifB-co (0.93 mM Fe). Bottom right: anaerobic vial with pure NifX/NifB-co (0.85 mM Fe).

Two methods were used to produce NifX/NifB-co. In method 1, ^{57}Fe-enriched purified NifB-co preparations were obtained from *Klebsiella oxytoca* cells derepressed for nitrogenase.[3] *Azotobacter vinelandii* NifX was obtained from recombinant *E. coli* cells.[5] NifX/NifB-co complexes were prepared in vitro under reducing conditions (2 mM dithionite) as in Ref. [5] and concentrated to 2 mM ^{57}Fe in an Amicon cell equipped with a YM10 membrane. In method 2, to avoid possible artifacts derived from NifB-co isolation or from

[*] Prof. Dr. Y. Guo,[+] Prof. Dr. E. L. Bominaar
Department of Chemistry, Carnegie Mellon University
4400 Fifth Ave, Pittsburgh, PA 15213 (USA)
E-mail: ysguo@andrew.cmu.edu
eb7g@andrew.cmu.edu
Dr. C. Echavarri-Erasun,[+] Dr. M. Demuez, Dr. E. Jiménez-Vicente, Prof. Dr. L. M. Rubio
Centro de Biotecnología y Genómica de Plantas
Universidad Politénica de Madrid (UPM)—Instituto Nacional de Investigación y Tecnología Agraria y Alimentaria (INIA)
Campus Montegancedo UPM, 28223-Pozuelo de Alarcón, Madrid (Spain)
E-mail: lm.rubio@upm.es
[+] These authors contributed equally to this work.
Supporting information and the ORCID identification number(s) for the author(s) of this article can be found under: http://dx.doi.org/10.1002/anie.201606447.

NifX/NifB-co complex formation in vitro with method 1, we generated a *K. oxytoca* strain in which FeMo-co biosynthesis was interrupted at the level of NifEN and a glutathione-S-transferase (GST)-NifX fusion protein was overexpressed, leading to the in vivo accumulation of ^{57}Fe-enriched NifX/NifB-co complex that was purified by affinity chromatography (method 2, Supporting Information, Figures S1 and S2). In vivo generated NifX/NifB-co contained an average of 7.4 Fe atoms mol^{-1} of NifX (average from 10 preparations) and was active in the FeMo-co biosynthesis and nitrogenase activation assay (Figure 1C).

The zero-field Mössbauer spectrum of in vivo formed ^{57}Fe-enriched NifX/NifB-co (method 2) recorded at 4.2 K exhibited two quadrupole doublets (Figure 2A). For the minor doublet (doublet II), only the high-energy absorption line is resolved, while the low-energy line is hidden under the low-energy line of the major doublet (doublet I). By using a Fourier transform technique to eliminate the ^{57}Co source linewidth contribution to the spectrum (Supporting Information, Figure S3),[8,9] we showed that the low-energy lines of doublets I and II coincide. The fit of the spectrum in Figure 2A gave the isomer shifts and quadrupole splittings of $\delta_I = 0.41$ mm s^{-1}, $\Delta E_{QI} = 1.04$ mm s^{-1} (doublet I), $\delta_{II} = 0.62$ mm s^{-1}, $\Delta E_{QII} = 1.46$ mm s^{-1} (doublet II), and a I:II absorption ratio of circa 3:1 (Table 1). The isomer shift has been used as a reliable oxidation state indicator in Fe–S cluster studies.[10] The isomer shift of doublet I is almost identical to the averaged isomer shift of FeMo-co from *A. vinelandii* ($\delta_{av} = 0.41$ mm s^{-1} at 4.2 K),[11] of FeV-co from *A. vinelandii* ($\delta_{av} = 0.39$ mm s^{-1} at 80 K),[12] and of FeFe-co from *Rhodobacter capsulatus* ($\delta_{av} = 0.40$ mm s^{-1} at 77 K).[13] The isomer shift of doublet II is in the range of the isomer shifts of the ferrous sites in Fe–S clusters.[10] The quadrupole splittings of the two doublets are temperature dependent (Table 1). Moreover, at higher temperatures, the absorption area ratio between doublets I and II changed from 3:1 (at 4.2 K) to > 4:1 (at 150 K). As the Mössbauer absorption area is proportional to the Lamb–Mössbauer factor, f_{LM}, the observed ratio change implies that the f_{LM} for the Fe sites of the two quadrupole doublets have different temperature dependences (Figure 2A,B and Table 1). This observation suggests that the Fe sites represented by doublet I are bound more tightly than those represented by doublet II. Identical Mössbauer spectra with a I:II absorption ratio of approximately 3:1 at 4.2 K were also observed for the NifX/NifB-co sample prepared in vitro (method 1, Supporting Information, Figures S5 and S6 and Table 1). The similarity in the results obtained with methods 1 and 2 strongly suggests that doublets I and II do not belong to different Fe–S clusters in the samples but are associated with distinct sites of a single NifB-co cluster. Distinct iron sites with different temperature dependences of f_{LM} have also been observed in the P-cluster of the MoFe protein.[14] Because the Fe-site ratio determined from the 4.2 K spectra was found to be more reliable than the ratios obtained at higher temperatures, the 4.2 K ratio was used to determine the relative abundance of the spectroscopically distinct Fe sites in NifB-co.

The 3:1 absorption ratio constrains the number of Fe atoms in NifX/NifB-co. Chemical analysis showed that there are circa 7.4 Fe atoms mol^{-1} NifX, hence NifX/NifB-co is most likely an 8-Fe cluster with 6 Fe atoms represented by doublet I and 2 Fe atoms by doublet II. Previous EXAFS and NRVS studies suggested that NifX/NifB-co prepared by method 1 contained at least 6 Fe sites that were best described as the central [6Fe–9S–X] moiety of FeMo-co (X is the interstitial atom, later identified as C^{4-}),[7,15,16] although 7-Fe and 8-Fe

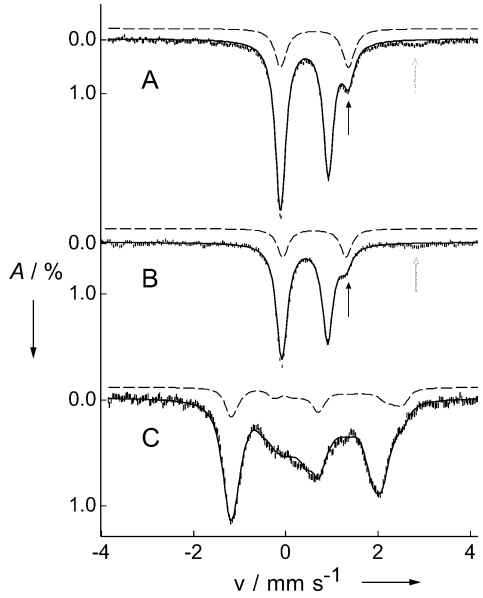

Figure 2. Mössbauer spectra of NifX/NifB-co prepared by the in vivo method (method 2). A) and B) are zero-field spectra recorded at 4.2 K and 150 K, respectively. C) Spectrum recorded at 4.2 K with 8.0 T applied magnetic field parallel to the γ radiation. Black solid lines are spectral simulations using the parameters in Table 1. Black dashed lines are spectral simulations of doublet II. The black arrows indicate the high-energy absorption line of doublet II, and the grey arrows indicate the high energy absorption line of ferrous impurity representing approximately 4% of the total iron in the sample (see the Supporting Information, Figure S4).

Table 1: Mössbauer parameters of ^{57}Fe-enriched NifX/NifB-co.[a]

T [K]		Method 1		Method 2	
		Doublet I	Doublet II	Doublet I	Doublet II
4.2	δ [mm s^{-1}][b]	0.41(1)	0.58(1)	0.41(1)	0.62(1)
	ΔE_Q [mm s^{-1}][c]	+1.02(2)	+1.55(3)	+1.04(2)	+1.46(3)
	Area [%]	73(2)	26(2)	71(2)	24(2)
	Γ [mm s^{-1}][d]	0.27	0.30	0.28	0.31
150	δ [mm s^{-1}][b]	0.42(1)	0.59(1)	0.41(1)	0.63(1)
	ΔE_Q [mm s^{-1}][c]	0.91(2)	1.34(3)	1.00(2)	1.33(3)
	Area [%]	85(2)	15(2)	78(2)	18(2)
	Γ [mm s^{-1}][d]	0.28	0.33	0.31	0.32

[a] The numbers in parentheses are uncertainties of the least significant digit. [b] Isomer shifts are quoted relative to iron metal at 298 K. Isomer shifts obtained in the experiments are not subject to second-order Doppler shifts due to the instrumental setup, in which the source and the sample were kept at the same temperature. [c] ΔE_Q signs were determined from the 8.0 T spectrum. [d] The linewidths used in the spectral simulations.

models were not ruled out. The current Mössbauer data provide evidence supporting an 8-Fe cluster for NifX/NifB-co. The observation of two distinct types of Fe sites in NifB-co is unique: six out of the eight irons in NifB-co have delocalized valences, while the remaining two have localized valences. NifB-co is different from FeMo-co, in which all irons have delocalized valences.[11]

To determine the spin state of NifX/NifB-co, high-field Mössbauer measurements were performed. Figure 2C shows the 8.0 T spectrum of ^{57}Fe-enriched NifX/NifB-co. The simulation reveals that both quadrupole doublets observed in the zero-field spectrum are diamagnetic ($S=0$), which is consistent with previous EPR studies of NifX/NifB-co.[3,5] From Figure 2C, the sign of ΔE_Q as well as the asymmetry parameters for the two quadrupole doublets have been determined, yielding $\Delta E_Q > 0$ and $\eta_I = 0.7$ (doublet I), $\eta_{II} = 0.2$ (doublet II).

The Mössbauer parameters for NifX/NifB-co guided the DFT studies (for details, see the Supporting Information). Table 2 lists our attempts to determine the oxidation state of

Table 2: Isomer shifts from DFT[a] and Mössbauer spectroscopy for NifB-co.

Method	Oxidation State	δ [mm s^{-1}] Fe_T	δ [mm s^{-1}] Fe_{Eq}	Σ δ[b] [mm s^{-1}]
	$[2Fe_T^{3+}6Fe_{Eq}^{3+}9S^{2-}C^{4-}]^{2+}$	0.40	0.28	2.48
	$[2Fe_T^{2+}6Fe_{Eq}^{3+}9S^{2-}C^{4-}]^{0}$	0.56	0.29	2.86
DFT	$[2Fe_T^{2+}6Fe_{Eq}^{2.66+}9S^{2-}C^{4-}]^{2-}$	0.49	0.38	3.26
	$[2Fe_T^{2+}6Fe_{Eq}^{2.33+}9S^{2-}C^{4-}]^{4-}$	**0.41**	**0.49**	**3.76**
	$[2Fe_T^{2+}6Fe_{Eq}^{2+}9S^{2-}C^{4-}]^{6-}$	0.38	0.70	4.96
	$[2Fe_T^{3+}6Fe_{Eq}^{3+}6S^{2-}3(HS)^{-}C^{4-}]^{5+}$	0.55	0.36	3.28
	$[2Fe_T^{2+}6Fe_{Eq}^{3+}6S^{2-}3(HS)^{-}C^{4-}]^{3+}$	0.72	0.35	3.52
DFT	**$[2Fe_T^{2+}6Fe_{Eq}^{2.66+}6S^{2-}3(HS)^{-}C^{4-}]^{1+}$**	**0.62**	**0.41**	**3.71**
	$[2Fe_T^{2+}6Fe_{Eq}^{2.33+}6S^{2-}3(HS)^{-}C^{4-}]^{1-}$	0.52	0.52	4.13
	$[2Fe_T^{2+}6Fe_{Eq}^{2+}6S^{2-}3(HS)^{-}C^{4-}]^{3-}$	_[c]	_[c]	_[c]
Mb[d]	[8Fe nS^{2-} $mH^{+}X]^{?}$	0.62	0.41	3.70

[a] The results were obtained for B3LYP/TZVP optimized structures of imposed D_{3h}-symmetric clusters (Figure 3 and Supporting Information, Figure S8) for the broken-symmetry state $Fe_T\uparrow 3(Fe_{Eq}\downarrow)3(Fe_{Eq}\uparrow)Fe_T\downarrow$; the δ values were subsequently evaluated from single-point B3LYP/6-311g calculations for B3LYP/TZVP optimized structures. The calibration used for evaluating δ from the DFT results has been described in the Supporting Information. Fe_T, terminal iron; Fe_{Eq}, equatorial iron. [b] Sum over the isomer shifts of the eight irons in NifB-co is calculated as $\Sigma\delta = 6\delta(Fe_{Eq}) + 2\delta(Fe_T)$. [c] No satisfactory state was obtained. [d] Mb: Mössbauer.

the NifB-co cluster using D_{3h}-symmetric unprotonated [8Fe–9S–C] and protonated [8Fe–6S–3(μ_2-SH)–C] clusters. The structural model and electronic state used in the DFT calculations are illustrated in Figure 3 in the case of the [8Fe–9S–C] cluster, and the Supporting Information Figure S8 for the protonated cluster. As NifB-co has a diamagnetic electronic ground state (both as-isolated and in the complex with NifX), the oxidation states of the 8-Fe cluster model have been changed, starting from the all-ferric cluster, in 2e$^-$ reduction steps using the broken symmetry (BS) state.[17,18] All the models tested had two types of iron with 3:1 ratio (six equatorial irons, Fe_{Eq}, and two terminal irons Fe_T),

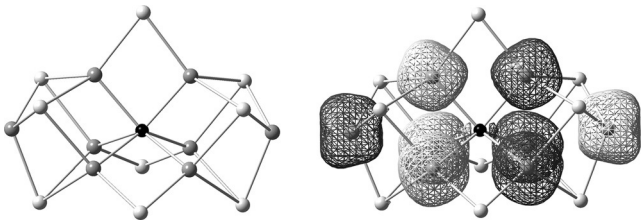

Figure 3. Left: DFT optimized structure for the $[2Fe_T^{2+}6Fe_{Eq}^{2.66+}9S^{2-}C^{4-}]^{2-}$ cluster. S = light grey, Fe = dark grey, and C = black. Right: Spin density plot for the broken symmetry state with $M_S = 0$ for which the structure was optimized. Net spin-up density (dark mesh) and net spin-down density (white mesh).

consistent with the Mössbauer results. The calculated δ values generally follow the trend that a lower iron oxidation state (Fe^{2+} vs. Fe^{3+}) gives a higher δ value. With no information available regarding the spin ordering in NifB-co, the ordering adopted in the BS-DFT calculations (Figure 3) may not yield accurate results for the individual iron sites. However, the sum of δ values (Σ δ in Table 2) is expected to be an indicator for the oxidation state of the NifB-co cluster. Among all the oxidation states calculated for the D_{3h} 8-Fe cluster model, the unprotonated (−4) state with a formal $6Fe^{2+}2Fe^{3+}$ configuration ($[2Fe_T^{2+}6Fe_{Eq}^{2.33+}9S^{2-}C^{4-}]^{4-}$) and the protonated (+1) state with a $4Fe^{2+}4Fe^{3+}$ configuration ($[2Fe_T^{2+}6Fe_{Eq}^{2.66+}6S^{2-}$-$3(HS)^{-}C^{4-}]^{1+}$) provide the best agreements with the Mössbauer data (see the Supporting Information).

In the FeMo-co biosynthetic pathway, the NifB-co produced by NifB binds to the NifEN scaffold protein and is further modified in a series of reactions that include the incorporation of Mo and homocitrate to yield FeMo-co.[19] The first of such reactions is the conversion of NifB-co into the VK-cluster,[5] a Mo-free, homocitrate-free paramagnetic Fe–S cluster capable of undergoing two-electron redox transitions. The atomic structure of the VK-cluster (renamed as L-cluster by the authors) inside the *A. vinelandii* NifEN protein has been recently solved;[20] its electron density map was consistent with a [8Fe–9S] cluster closely resembling the inorganic [7Fe–Mo–9S–C] core of FeMo-co, although the 2.6 Å resolution did not allow the observation of the interstitial C atom. The present evidence, which supports that NifB-co is an 8-Fe cluster, suggests that VK-cluster formation requires no additional Fe and that NifB-co and the VK-cluster are equivalent in terms of nuclearity. This interpretation is intriguing because NifB-co is a diamagnetic cluster, whereas the VK-cluster exhibits paramagnetism in both the reduced and the oxidized states.[5] This implies that these clusters are in different oxidation states and/or have different spin ordering schemes. Further experiments are underway to determine the origin of the spectroscopic differences between NifB-co and the VK-cluster and its relevance to the FeMo-co biosynthesis.

In conclusion, the first complex Fe–S cluster intermediate in the FeMo-co biosynthetic pathway, NifB-co, exhibits two quadrupole doublets with an absorption area ratio of 3:1 at 4.2 K. Both doublets are diamagnetic, consistent with irons belonging to the same $S = 0$ spin system. By comparing with previous Mössbauer experiments on FeMo-co, FeFe-co, and

FeV-co (particularly the isomer shifts), along with DFT calculations within the broken symmetry formalism on a D_{3h}-symmetric 8-Fe cluster model, we conclude that NifB-co is best described as an 8-Fe cluster with either formal ($6Fe^{2+}$–$2Fe^{3+}$) or ($4Fe^{2+}$–$4Fe^{3+}$) configurations. Two of the irons (Fe_T) are more loosely bound than the remaining six (Fe_{Eq}) based on the difference in the temperature dependence of the Lamb–Mössbauer factor, f_{LM}, as anticipated for the capping irons in the 8-Fe cluster.

Acknowledgements

We thank Elena Gonzalez de Heredia for constructing pRHB731. We also thank Prof. Eckard Münck for valuable discussions. This work was supported by ERC Starting Grant 205442 (L.M.R.), MINECO BIO2014-59131-R Grant (L.M.R.). Y. G. acknowledges the financial support from Carnegie Mellon University.

Keywords: biosynthesis · iron–molybdenum cofactors · metalloproteins · mössbauer spectroscopy · nitrogenases

How to cite: *Angew. Chem. Int. Ed.* **2016**, *55*, 12764–12767
Angew. Chem. **2016**, *128*, 12956–12959

[1] L. M. Rubio, P. W. Ludden, *Annu. Rev. Microbiol.* **2008**, *62*, 93.
[2] L. Curatti, P. W. Ludden, L. M. Rubio, *Proc. Natl. Acad. Sci. USA* **2006**, *103*, 5297.
[3] V. K. Shah, J. R. Allen, N. J. Spangler, P. W. Ludden, *J. Biol. Chem.* **1994**, *269*, 1154.
[4] R. M. Allen, R. Chatterjee, P. W. Ludden, V. K. Shah, *J. Biol. Chem.* **1995**, *270*, 26890.
[5] J. A. Hernandez, R. Y. Igarashi, B. Soboh, L. Curatti, D. R. Dean, P. W. Ludden, L. M. Rubio, *Mol. Microbiol.* **2007**, *63*, 177.
[6] Y. Hu, M. C. Corbett, A. W. Fay, J. A. Webber, K. O. Hodgson, B. Hedman, M. W. Ribbe, *Proc. Natl. Acad. Sci. USA* **2006**, *103*, 17119.
[7] S. J. George, R. Y. Igarashi, Y. Xiao, J. A. Hernandez, M. Demuez, D. Zhao, Y. Yoda, P. W. Ludden, L. M. Rubio, S. P. Cramer, *J. Am. Chem. Soc.* **2008**, *130*, 5673.
[8] C. D. M. Ure, P. A. Flinn in *Mössbauer Eff. Methodol* (Ed.: I. J. Gruverman), Springer, New York, **1971**, p. 245.
[9] W. R. Dunham, L. J. Harding, R. H. Sands, *Eur. J. Biochem.* **1993**, *214*, 1.
[10] H. Beinert, R. H. Holm, E. Münck, *Science* **1997**, *277*, 653.
[11] S. J. Yoo, H. C. Angove, V. Papaefthymiou, B. K. Burgess, E. Münck, *J. Am. Chem. Soc.* **2000**, *122*, 4926.
[12] N. Ravi, V. Moore, S. G. Lloyd, B. J. Hales, B. H. Huynh, *J. Biol. Chem.* **1994**, *269*, 20920.
[13] E. Krahn, B. J. R. Weiss, M. Kröckel, J. Groppe, G. Henkel, S. P. Cramer, A. X. Trautwein, K. Schneider, A. Müller, *J. Biol. Inorg. Chem.* **2002**, *7*, 37.
[14] P. A. McLean, V. Papaefthymiouv, W. H. Orme-Johnson, E. Münck, *J. Biol. Chem.* **1987**, *262*, 12900.
[15] T. Spatzal, M. Aksoyoglu, L. Zhang, S. L. A. Andrade, E. Schleicher, S. Weber, D. C. Rees, O. Einsle, *Science* **2011**, *334*, 940.
[16] K. M. Lancaster, M. Roemelt, P. Ettenhuber, Y. Hu, M. W. Ribbe, F. Neese, U. Bergmann, S. DeBeer, *Science* **2011**, *334*, 974.
[17] L. Noodleman, *J. Chem. Phys.* **1981**, *74*, 5737.
[18] T. Lovell, J. Li, T. Liu, D. A. Case, L. Noodleman, *J. Am. Chem. Soc.* **2001**, *123*, 12392.
[19] J. A. Wiig, Y. Hu, M. W. Ribbe, *Proc. Natl. Acad. Sci. USA* **2011**, *108*, 8623.
[20] J. T. Kaiser, Y. Hu, J. A. Wiig, D. C. Rees, M. W. Ribbe, *Science* **2011**, *331*, 91.

Received: July 3, 2016
Published online: September 9, 2016

